Understanding the electromagnetic field in an MRI scanner

Jan Bouwe van den Berg[*] *Nico van den Berg*[†] *Bob van den Bergen*[†]
Alex Boer[‡] *Fokko van de Bult*[§] *Sander Dahmen*[‡] *Katrijn Frederix*[¶]
Yves van Gennip[‖] *Joost Hulshof*[*] *Hil Meijer*[**] *Peter in 't Panhuis*[‖]
Chris Stolk[**] *Rogier Swierstra*[‡] *Marco Veneroni*[‖] *Erwin Vondenhoff*[‖]

Abstract

In this note, we study the magnetic field pattern in an MRI scanner, in order to ultimately improve the resolution of the image. We model the situation in 2-D, with a simplified model for the patient, consisting of two regions bounded by ellipses with constant dielectric properties. The solution to the Maxwell equations is described in terms of two different bases: Bessel and Mathieu functions. By expansions in Bessel (cylindrical) modes, that are matched at the boundaries, the magnetic field can be computed in a few seconds on a PC or Mac. By optimizing the distribution of antenna currents the homogeneity of the magnetic field can be improved.

Key words: MRI scanner, Maxwell equations, Bessel functions, Mathieu functions

1 Introduction

In an MRI scanner a patient is placed in a strong constant magnetic field. We give a brief heuristic (mixed classical and quantum-mechanical) description of the main physical process. The magnetic field aligns all dipoles (for practical purposes, the spin-1/2 hydrogen nuclei) in the patient's body parallel or anti-parallel to this field. However, this alignment is not perfect and therefore the dipoles

[*]Vrije Universiteit, Amsterdam
[†]UMC, Utrecht
[‡]Universiteit Utrecht
[§]Universiteit van Amsterdam
[¶]Katholieke Universiteit Leuven, Belgium
[‖]Technische Universiteit Eindhoven
[**]Technische Universiteit Twente

precess around the radial axis of the field with a typical frequency, called the Larmor frequency, proportional to the size of the external field.

Subsequently, electromagnetic waves are created in the cavity of the scanner (by sending currents through antennas placed inside the MRI scanner), which excite the hydrogen dipoles. The frequency of these waves is chosen to be the Larmor frequency to maximize the number of excitations. The electromagnetic waves temporarily cause some of the dipoles to leave their parallel/anti-parallel state, and when the wave field subsides, these dissidents "fall back" to a parallel/anti-parallel state. This causes the emission of a photon, a scanner detects these photons, and from this information a computer constructs an image of the object or person in the MRI scanner. What is effectively measured here, is the density of dipoles with fixed Larmor frequency — in practice, hydrogen nuclei.

As the strength of the magnetic field increases, so does the Larmor frequency, and hence the frequency of the electromagnetic waves. Advances in superconducting magnet design and in MRI technology have increased the field strength to such an extent that nowadays the wavelength of the electromagnetic waves is of the order of the size of the patient. This causes the field to be significantly altered from the field in an empty MRI scanner if a patient is inserted. Moreover, the homogeneity of the magnetic field is reduced. This has the disadvantage that the received image is distorted: it will show too many hydrogen atoms where the induced field is big and too few where the field is small. Moreover, the induced electric field may lead to significant currents which heat up the patient.

Therefore, the question is how to create an induced electromagnetic field whose magnetic field is homogeneous and whose electric field is small. As constraints we assume the geometry of the MRI scanner (i.e., size of the scanner, size of the patient, location of the antennas etc.) to be given, and we are only allowed to change the phases and amplitudes of the currents through the antennas. In practice, changing the size of the scanner would be prohibitively expensive, and one cannot really change the size of the patients either. However, the antennas could be moved around a bit, but for mathematical simplicity we do not consider this option here.

To answer this question we first have to be able to find a "simple" expression for the induced field generated by the antennas when a given current runs through them. After some introductory remarks about electromagnetic waves in Sections 2 and 3 we present two methods to obtain an approximation of the induced field. In Section 4 we discuss an expression using Bessel functions. This has the advantage that Bessel functions are well-known and many good numerical packages exist for them. In Section 5 we consider an option using Mathieu functions, which are less easy to work with numerically, but fit the geometry of the situation better. Finally, in Section 6, we consider how to optimize the currents, given the fields generated by the individual antennas, such as to maximize the homogeneity of the induced magnetic field.

2 Geometric considerations

The outer cylinder of the MRI scanner itself has, to good approximation, a rotation and translation symmetry along the central axis. We choose coordinates so that the z-direction corresponds to the translation symmetry, and $x = y = 0$ on the central axis. The edge of the scanner will therefore be a circle at radius r (typically $r \approx 35$ cm).

We consider a cross-section of the patient's abdomen. In this region the patient is modeled by two (confocal) ellipses. The outer one denotes a surrounding fat layer, while the inner one denotes the inside of the patient with organs and muscles and bones. In each layer we consider the electromagnetic properties to be constant; in particular, we use an average of the electromagnetic

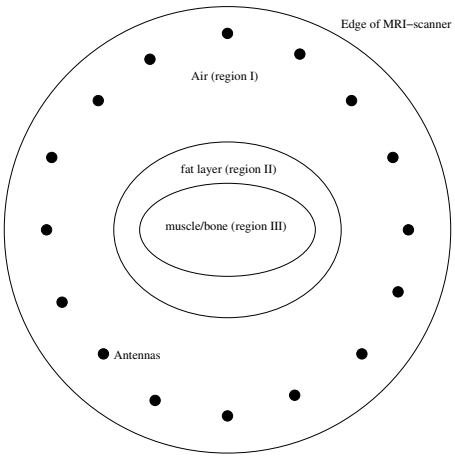

Figure 2.1: Cross-section of the MRI-scanner.

properties of the different tissues in the inside layer. The typical size of the inner ellipse is an outer radius of 15 cm and an eccentricity of 0.85, while the outer ellipse can vary a lot, but is generally not more than 10 cm thick.

Finally, the antennas are modeled as point/line sources located in a circle at a distance of a few centimeters from the edge of the scanner. The currents running through the antennas will have constant frequency, and we assume that the electromagnetic properties of the different layers are time-independent for this fixed frequency.

3 Maxwell equations

We will show that in the case at hand, the Maxwell equations, which describe the electromagnetic field in general, reduce to a single Helmholtz equation in each of the three regions. The theory used is well-known, so we shall go through the derivation rapidly. For references on our notation, consult [1].

We begin by writing down the Maxwell equations for the four fields: the electric field E, the magnetic field B, the so-called displacement field D and the auxiliary field H[1]. The free charge and the current are denoted by ρ and J respectively.

$$\nabla \cdot B = 0, \qquad \nabla \times E + \frac{\partial B}{\partial t} = 0, \tag{3.1a}$$

$$\nabla \cdot D = \rho, \qquad \nabla \times H - \frac{\partial D}{\partial t} = J. \tag{3.1b}$$

The equations on the first line are known as the *homogeneous Maxwell equations*, and are universally valid. Those on the second line – the *inhomogeneous Maxwell equations* – depend on free charges and currents, and on the different materials in our system.

By assumption, our materials are linear and isotropic, which means that, in each region, D and H are scalar multiples of E and B respectively. We write $D = \epsilon E$ and $H = \mu B$, where the dielectric

[1] Although different authors may use different names for these fields, there is consensus about the symbols.

constant ϵ and the magnetic permeability μ are constants of the materials in the different regions. In the situation of the MRI scanner, μ is constant throughout, and equal to μ_0, the permeability of the vacuum.

Next, we discuss the boundary conditions. Since the conductivity in the inner regions (patient) is much smaller than that of the metal cylinder, the losses in the latter will be small, hence we will assume it to be superconducting. Further, we will neglect the penetration depth of the current in the metal. Let n be a vector normal to the boundary between two media 1 and 2, and let D_i, E_i, $i = 1, 2$, be the displacement and electric fields, respectively, then

$$n \cdot (D_1 - D_2) = \Sigma, \qquad n \times E_1 = n \times E_2.$$

Here Σ is the free surface charge between the media. In particular, the *tangential* component of E vanishes on the outer boundary (i.e., the MRI scanner itself). The boundary conditions for B and H are similar, and, since μ is constant, they imply that B is continuous on the entire domain.

The two inhomogeneous Maxwell equations (3.1b) imply the conservation law

$$\frac{\partial \rho}{\partial t} + \nabla \cdot J = 0.$$

In the current term J, we must distinguish between the externally imposed current J_{ext}, and the current J_{ind} induced in the medium by the electric field. We assume that the induced currents are governed by Ohm's law, i.e. $J_{\text{ind}} = \sigma E$, where σ is the conductivity of the medium. We note that different sources approach this in different ways: some include the induced currents in the J, others redefine ϵ, which is then commonly referred to as the complex permittivity. The externally imposed current is assumed to consist of N line sources, located at positions (x_l, y_l) to be specified later:

$$J_{\text{ext}} = J_{\text{ext}}(x, y, t) = \sum_{l=1}^{N} \begin{pmatrix} 0 \\ 0 \\ I_l \exp(i\omega t)\delta(x - x_l)\delta(y - y_l) \end{pmatrix}, \tag{3.2}$$

where the constants I_l determine the amplitude and the phase of the currents (obviously, in reality all the physical quantities are real, but this complex formalism simplifies the formulas).

The homogeneous Maxwell equations (3.1a) imply the existence of potential functions: a *vector potential* A and a *scalar potential* Φ. They are related to the electromagnetic fields via

$$B = \nabla \times A, \qquad E = -\nabla\Phi - \frac{\partial A}{\partial t}. \tag{3.3}$$

We note that A and Φ are not uniquely defined: if (A, Φ) are potentials, then one can check that $(A + \nabla f, \Phi - \frac{\partial f}{\partial t})$ are potentials of the same fields, for any function f. This non-uniqueness, called *gauge*-freedom, can be used to impose some conditions on A and Φ. There are several choices for this, but we will use the so called Lorenz[2]-gauge:

$$\nabla \cdot A + \frac{1}{c^2}\frac{\partial \Phi}{\partial t} = 0, \qquad \text{where} \quad \frac{1}{c^2} = \epsilon\mu.$$

This gauge is chosen so that the inhomogeneous equations would separate if the domain were homogeneous, which our domain is not; nevertheless, we stick with the Lorenz gauge.

[2] Although often erroneously called Lorentz gauge, supposedly after Hendrik Lorentz, it was in fact Ludwig Lorenz who first published the idea.

Based on the symmetries of the problem, the expression (3.2) for J_{ext}, and physical intuition, we now take the *Ansatz*

$$\Phi = 0, \qquad \text{and} \qquad A = \begin{pmatrix} 0 \\ 0 \\ A_z(x, y, t) \end{pmatrix}.$$

For notational convenience, we write x for the pair (x, y), and we replace A_z by A, hence $A_z(x, y, t)$ becomes $A(x, t)$, with $x \in \mathbb{R}^2$. The governing equation for the vector potential is

$$\epsilon\mu \frac{\partial^2 A}{\partial t^2} = \Delta A + \mu J, \tag{3.4}$$

which is to hold globally, i.e., A is continuously differentiable throughout the domain (in particular across the boundaries between the regions), except at the antennas, where singularities occur. As boundary condition we take $A = 0$ on the outer boundary.

In view of the time dependence of the currents through the antennas, we expect waves of fixed frequency ω. This means that all functions under consideration (and in particular A) are a product of a function that depends only on space, and $e^{i\omega t}$. The spatial part of a function will be denoted by the same letter as the function itself, e.g., the electric field is from now on of the form $Ee^{i\omega t}$. We thus replace $\frac{\partial A}{\partial t}$ by $i\omega A$ and $\frac{\partial^2 A}{\partial t^2}$ by $-\omega^2 A$.

Recalling that

$$J_{\text{ind}} = \sigma E = -\frac{\partial A}{\partial t} = -i\omega A$$

and by combining (3.4) and (3.2) we obtain an elliptic (Helmholtz) equation, for $\vec{x} \in \Omega \subset \mathbb{R}^2$,

$$\left(\Delta + \zeta^2\right) A = -\sum_{l=1}^{N} c_l \delta(\vec{x} - \vec{x}_l), \qquad A|_{\partial\Omega} = 0, \tag{3.5}$$

for the nonzero component of the vector potential. Here

$$c_l = \mu I_l,$$

and

$$\zeta^2 = \epsilon\mu\omega^2 - i\sigma\omega$$

is (a complex) constant on each of the regions. We will also use the notation $\zeta_k^2 = \epsilon_k \mu_0 \omega^2 - i\sigma_k \omega$ for the three regions $k = 1, 2, 3$. Note that to good approximation $\epsilon_1 = \epsilon_0$, the dielectric constant of vacuum/air.

Equation (3.5) indeed has a (unique) solution, from which we can recover the fields B and E using (3.3). It is easily checked that these fields then satisfy the Maxwell equations as well as the boundary conditions, hence they represent a solution to our original problem. In fact, general PDE theory for Maxwell equations implies that it is the unique solution. We are thus left with the task of finding the solution of the Helmholtz equation (3.5).

4 Cylindrical modes

Within each region the coefficients ϵ, σ, and μ are constant. For the constant coefficient PDE, an infinite number of solutions can easily be found by separation of variables. Since the Helmholtz equation (3.5) is linear, with an inhomogeneous right-hand side, we solve the equation for one antenna at a time, and we may restrict our attention to $c_l = 1$. Based on this, the strategy in this section will be as follows:

1. In region I (see Figure 2.1 for the geometry of the various regions), write $A = \tilde{A} + F$, with F a fundamental solution. The function $\tilde{A}$ then satisfies a homogeneous PDE, with inhomogeneous boundary conditions.

2. For each of the regions, find a set of basis functions that satisfy the homogeneous PDE.

3. Write A and $\tilde{A}$ as a finite linear combination of the basis functions in each region. Each linear combination automatically satisfies the PDE. Choose the coefficients such that the boundary conditions are satisfied, or at least as well as possible, since only a finite number of modes can be used in practice.

We will use polar coordinates (even if the domain and the different regions (as well as the patient) are elliptic). Furthermore, we drop the tilde (on A in region I) from the notation.

The fundamental solution $F = F(\vec{x}, \vec{x}_l)$ satisfies

$$(\Delta + \zeta_1^2)F = -\delta(\vec{x} - \vec{x}_l),$$

where $\zeta_1 = \omega\sqrt{\epsilon_0\mu_0}$ as explained in the previous section. The solution is readily given by

$$F = -\frac{1}{4}Y_0(\zeta_1|\vec{x} - \vec{x}_l|),$$

where Y_0 is the 0-th order Bessel function of the second kind (notice that F is not uniquely determined since any smooth solution of the homogeneous PDE can be added to it). With the source at the antenna position, we have

$$F = -\frac{1}{4}Y_0(\zeta_1\,\rho),$$

where $\rho(r,\theta) = r^2 + R_{\text{ant}}^2 - 2R_{\text{ant}}r\cos(\theta - \theta_{\text{ant}})$ is the distance to the antenna, which is positioned at $(R_{\text{ant}}, \theta_{\text{ant}})$, in polar coordinates.

To find the basis functions we use separation of variables in polar coordinates, which can be found in many textbooks on PDEs. Substituting the *Ansatz* $A(r,\theta) = R(r)\Theta(\theta)$, we find that Θ must satisfy the eigenvalue problem

$$\Theta'' + \lambda\Theta = 0, \qquad \Theta \text{ is } \pi\text{-periodic},$$

with solutions $\Theta = e^{in\theta}$, $\lambda = n^2$, $n \in \mathbb{Z}$, while R must satisfy the equation

$$\frac{d^2R}{dr^2} + \frac{1}{r}\frac{dR}{dr} - \frac{n^2}{r^2}R + \zeta^2 R = 0.$$

This equation has two linearly independent solutions for each n:

$$J_n(\zeta\, r) \quad \text{and} \quad Y_n(\zeta\, r),$$

where J_n and Y_n are the Bessel functions of order n of the first and second kind, respectively. The basis functions are therefore $\phi_{k,n}(r)e^{in\theta}$ and $\psi_{k,n}(r)e^{in\theta}$, with

$$\phi_{k,n}(r) = \kappa_{k,n}\, J_n(\zeta\, r),$$
$$\psi_{k,n}(r) = \tilde{\kappa}_{k,n}\, Y_n(\zeta\, r),$$

where $k = 1, 2, 3$ represents the region, and $\kappa_{k,n}$ and $\tilde{\kappa}_{k,n}$ are normalization constants.

In regions I, II and III we now use the following representation of the solution:

$$\begin{aligned}
A_1(r,\theta) &= F(\rho) + \sum_{j=-n_1}^{n_1} a_{1,j}\phi_{1,j}(r)e^{ij\theta} + \sum_{j=-\tilde{n}_1}^{\tilde{n}_1} b_{1,j}\psi_{1,j}(r)e^{ij\theta} \\
&\stackrel{\text{def}}{=} \Phi_1(r,\theta)\cdot a_1 + \Psi_1(r,\theta)\cdot b_1 \\
A_2(r,\theta) &= \sum_{j=-n_2}^{n_2} a_{2,j}\phi_{2,j}(r)e^{ij\theta} + \sum_{j=-\tilde{n}_2}^{\tilde{n}_2} b_{2,j}\psi_{2,j}(r)e^{ij\theta} \\
&\stackrel{\text{def}}{=} \Phi_2(r,\theta)\cdot a_2 + \Psi_2(r,\theta)\cdot b_2 \\
A_3(r,\theta) &= \sum_{j=-n_3}^{n_3} a_{3,j}\phi_{3,j}(r)e^{ij\theta} \\
&\stackrel{\text{def}}{=} \Phi_3(r,\theta)\cdot a_3,
\end{aligned}$$

where we define a_k and b_k, $k = 1, 2, 3$, to be column vectors containing the $a_{k,j}$ and $b_{k,j}$, and Φ_1 to be a row vector containing the functions $\phi_{1,j}(r)e^{ij\theta}$, and similarly for the other Φ's and Ψ's. The ψ's are omitted in region III, as they would cause an undesirable pole in the solution. The choice of the number of basis functions $n_k, k = 1, 2, 3$ and $\tilde{n}_k, k = 1, 2$ is discussed below.

Using the boundary conditions we try to match the solutions at the boundaries between the different regions and thus obtain the coefficients $a_{k,j}$ and $b_{k,j}$. These conditions are evaluated using a uniform distribution in the angle along the cavity (C) and ellipses (E_1 and E_2). This leads to the following over-determined system

$$\begin{pmatrix}
\Phi_1|_C & \Psi_1|_C & 0 & 0 & 0 \\
\Phi_1|_{E_1} & \Psi_1|_{E_1} & -\Phi_2|_{E_1} & -\Psi_2|_{E_1} & 0 \\
\frac{\partial\Phi_1}{\partial n}|_{E_1} & \frac{\partial\Psi_1}{\partial n}|_{E_1} & -\frac{\partial\Psi_2}{\partial n}|_{E_1} & -\frac{\partial\Psi_2}{\partial n}|_{E_1} & 0 \\
0 & 0 & \Phi_2|_{E_2} & \Psi_2|_{E_2} & -\Phi_3|_{E_2} \\
0 & 0 & \frac{\partial\Phi_2}{\partial n}|_{E_2} & \frac{\partial\Psi_2}{\partial n}|_{E_2} & -\frac{\partial\Phi_3}{\partial n}|_{E_2}
\end{pmatrix}
\begin{pmatrix} a_1 \\ b_1 \\ a_2 \\ b_2 \\ a_3 \end{pmatrix} =
\begin{pmatrix} -F|_C \\ -F|_{E_1} \\ -\frac{\partial F}{\partial n}|_{E_1} \\ 0 \\ 0 \end{pmatrix}. \tag{4.1}$$

Here $\frac{\partial}{\partial n}$ denotes the derivative in the direction normal to the boundary, and $\Phi_1|_C$ is the matrix with as its rows Φ_1 evaluated at (many) different points in C. To be precise, the elements of the matrix $\Phi_1|_C$ are given by $(\Phi_1|_C)_{j,k} = \phi_{1,-n_1-1+k}(r_j)e^{i(-n_1-1+k)\theta_j}$, in which (r_j, θ_j) are the points along C, and $k = 1, \ldots, 2n_1 + 1$. The other blocks in the matrix in (6) are defined similarly. The coefficients a_1, a_2, a_3, b_1, b_2 are obtained by solving the system (4.1) using a least squares approach.

The above algorithm was implemented in Matlab. In Figure 4.1 a plot of the field is given, for the following parameters. We set the outer cylinder to have a radius of 0.34 m, and the semi-axes of the ellipses to be 0.2 m, 0.125 m, and 0.175 m, 0.1 m for the outer and inner ellipse, respectively. The antenna was located at $\theta_{\text{ant}} = 0$, $R_{\text{ant}} = 0.315$ m, with unit current. Furthermore, we set the frequency at the Larmor frequency $\omega = 300$ MHz, and set material constants of $\epsilon_{\text{r}} = 5, \sigma = 0.076$, for the fatty layer, and $\epsilon_{\text{r}} = 5, \sigma = 0.4$ for the interior part of the body; see [5]. The number of the different modes used was $(20, 20, 13, 13, 13)$ for $(n_1, \tilde{n}_1, n_2, \tilde{n}_2, n_3)$. With lower orders very similar pictures were obtained. The computation of the coefficients was done in a few seconds on a PC. Evaluating all the basis functions to compute an image took more time, in the order of a minute depending on the resolution and the number of basis functions involved. The remaining errors in the boundary values were small, up to a few percent of the values of the fundamental solution on the circle and outer ellipse. A second example is shown in Figure 4.2, where we have two antennas, located at $\theta = 3\pi/8$ and $\theta = 11\pi/8$. The field is seen to have a hard time penetrating the body.

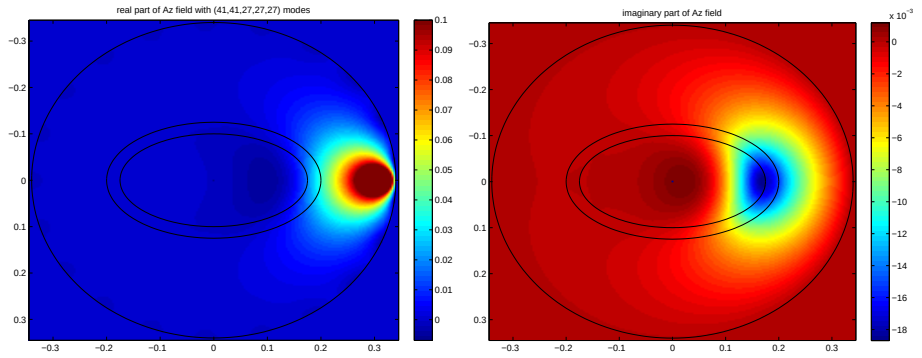

Figure 4.1: Real and imaginary part of the simulated A field

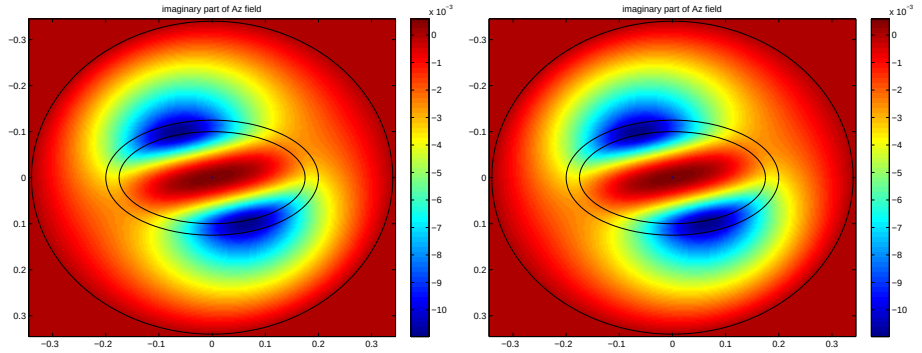

Figure 4.2: Real and imaginary part of the simulated A field, with two antennas.

Two remarks can be made about the numerics. First, the normalization is important, since Bessel functions are badly scaled on the domain of interest. Also, the rows in the system (4.1) that correspond to derivatives are normalized differently from the other rows. Second, the method breaks down because of rank deficiency of the matrix if the number of basis functions is too large. By choosing suitable normalization, quite a large number can be handled, whereas with a poor choice for normalization the rank deficiency occurs already for much smaller numbers of basis functions.

To conclude, the expansion in these cylindrical modes leads to a very fast algorithm. A comparison with results from finite-difference calculations could provide a final check of the results.

5 Mathieu functions

5.1 Elliptic coordinates

Let $\Omega \subset \mathbb{R}^n$ be a bounded open set, we now focus on the Helmholtz equation:

$$\Delta A + \zeta^2 A = 0, \quad \text{in } \Omega, \tag{5.1}$$

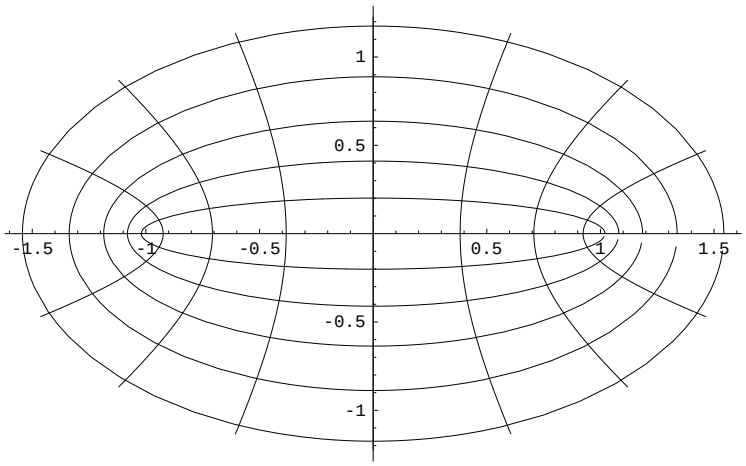

Figure 5.1: Elliptic coordinate grid: the ellipses are curves of constant ξ, the hyperboles curves of constant η.

for $\zeta \in \mathbb{C}$ specified in the previous sections. Since the specific domains we are interested in are elliptical, we introduce the elliptic coordinates, thus simplifying the form of the boundary conditions. We set

$$\begin{aligned} x &= a\cosh\xi\cos\eta, \\ y &= a\sinh\xi\sin\eta, \end{aligned}$$

where $2a$ is the distance between the foci, $\xi \geq 0$ and $\eta \in [-\pi, \pi)$. An impression of an elliptic coordinate grid is given in Figure 5.1.

Note that the ellipticity of the ellipse for given ξ equals $1/\cosh(\xi)$ and hence quickly becomes zero as $\xi \to \infty$. Equation (5.1) in elliptic coordinates becomes

$$\frac{2}{a^2(\cosh 2\xi - \cos 2\eta)}\left(\frac{\partial^2 A(\xi,\eta)}{\partial\eta^2} + \frac{\partial^2 A(\xi,\eta)}{\partial\xi^2}\right) + \zeta^2 A(\xi,\eta) = 0, \quad \text{in } \Omega. \tag{5.2}$$

Now we use the standard separation of variables technique, i.e., we look for a solution of the particular form $A(\xi,\eta) = X(\xi)Y(\eta)$. Then the partial differential equation (5.2) results in two linear ordinary differential equations:

$$\begin{cases} \dfrac{X''(\xi)}{X(\xi)} + \frac{1}{2}\zeta^2 a^2\cosh 2\xi &= \lambda, \\ \dfrac{Y''(\eta)}{Y(\eta)} - \frac{1}{2}\zeta^2 a^2\cos 2\eta &= -\lambda, \end{cases} \tag{5.3}$$

where λ is the separation constant. These equations are known as the *radial* and the *angular* Mathieu equations, respectively (see e.g. [2], [3], [4] and the references therein). Note that the radial equation can be obtained from the angular equation by the substitution $\eta = -i\xi$, hence the solutions of the radial equations are just those of the angular part with imaginary argument.

As any linear second order differential equation these equations have two independent solutions, and we can choose as basis of the solution space an even and an odd solution. Denote these by $C(\lambda, q, \eta)$ (even) and $S(\lambda, q, \eta)$ (odd) respectively, with (traditionally) $q = \frac{1}{4}\zeta^2 a^2$. The angular equation only has 2π-periodic solutions for specific values of λ, that are denoted by the two (q-dependent)

sequences $\lambda_k(q)$ ($k \geq 0$) and $\mu_k(q)$ ($k \geq 1$) respectively[3], called the characteristic values. The sequences $\lambda_k(q)$ and $\mu_k(q)$ are defined such that

$$C_k(q,\eta) = C(\lambda_k(q), q, \eta), \qquad S_k(q,\eta) = S(\mu_k(q), q, \eta),$$

are the 2π-periodic solutions, continuous in q, with $\lim_{q\to 0} C_k(q,\eta) = \cos(k\eta)$ and $\lim_{q\to 0} S_k(q,\eta) = \sin(k\eta)$. For $q = 0$ we have $\lambda_k = \mu_k = k^2$, but for $q \neq 0$ all λ_k and μ_k are generically different. For positive real q we have $\lambda_0 < \mu_1 < \lambda_1 < \mu_2 < \lambda_2 < \mu_3 < \ldots$, see [3].

The angular part of our solution $Y(\eta)$ should be 2π-periodic, hence we only retain these C_k's and S_k's as solutions for that part. Furthermore, using the eigenvalues λ_k and μ_k one can write down the radial solutions $X(\xi)$. Thus, we find that the system of equations (5.3) has the general solution:

$$\begin{aligned} A(\xi,\eta) = \sum_k &\Big(\alpha_k C(\lambda_k(q), q, -i\xi) + \beta_k S(\lambda_k(q), q, -i\xi)\Big) C_k(q,\eta) \\ &+ \Big(\gamma_k C(\mu_k(q), q, -i\xi) + \delta_k S(\mu_k(q), q, -i\xi)\Big) S_k(q,\eta), \end{aligned}$$

where the coefficients $\alpha_k, \beta_k, \gamma_k, \delta_k$ have to be determined in each of the specific domains by matching boundary conditions and imposing the correct symmetry and regularity for A.

In the domain containing the origin we must also ensure that the solution remains continuously differentiable on the line connecting the two focal points. For the even angular solutions, this implies that the derivative at $\xi = 0$ of the radial part must vanish (for it changes sign when passing the line between the focal points). For odd angular solutions, the value of the radial part itself must vanish on this line. More concretely, we lose the $S(\lambda_k, q, -i\xi)C_k(q,\eta)$ and $C(\mu_k, q, -i\xi)S_k(q,\eta)$ solutions on this domain, or alternatively $\beta_k = \gamma_k = 0$ on this domain.

5.2 Matching

It still remains to determine the constants α_k, β_k, γ_k and δ_k on all domains. Denote the solutions on the different domains by $A_1 + F$, A_2, A_3 for the domains I, II, and III, respectively, and the corresponding constants by $\alpha_{k,j}, \beta_{k,j}$ etc. for $j = 1, 2, 3$.[4] Here F is the solution in free space for the Helmholtz equation including the sources. We set ξ_1 to be the outer boundary of the scanner, and ξ_2 and ξ_3 to be the radii of the outer (resp. inner) ellipse of the patient. The boundary conditions then become

$$A_1 + F = 0 \qquad \text{on } \xi = \xi_1, \tag{5.4a}$$
$$A_2 = A_1 + F \qquad \text{on } \xi = \xi_2, \tag{5.4b}$$
$$A_3 = A_2 \qquad \text{on } \xi = \xi_3, \tag{5.4c}$$
$$\partial_\xi A_2 = \partial_\xi A_1 + \partial_\xi F \qquad \text{on } \xi = \xi_2, \tag{5.4d}$$
$$\partial_\xi A_3 = \partial_\xi A_2 \qquad \text{on } \xi = \xi_3, \tag{5.4e}$$

Heuristically, this will give us '5 sets' of conditions that can be used to determine the '10 sets' of constants $\alpha_{j,k}$ ($j = 1, 2, 3$), $\beta_{j,k}$ ($j = 1, 2$) etc..

Concerning condition (5.4a), as written down here we force our solution to vanish at an elliptical boundary, while the actual MRI scanner is circular. However, since the ellipticity of ξ-levels

[3] In the literature, these sequences are usually called $a_k(q)$ and $b_k(q)$, but in this paper we already use those symbols for different purposes.

[4] The indexing is a bit different from the one in the previous section.

decreases with ξ, the shape of the ellipse for ξ_1 is already close to a circle, and this will provide a rather good approximation. With a little extra work the matching can be performed on a circular interface as well.

The idea of the matching is to take a basis of the angular part of the solution on each interface, write the solutions on both sides in terms of this basis and then match the corresponding coefficients. When we started researching this method we hoped that the angular Mathieu functions in the different regions would give the same basis, so that we would not have to perform any base-change before the actual matching. This would reduce the boundary conditions to equations involving only 4 or 3 parameters each. However, as the functions C_k and S_k do depend on q, we were out of luck. This forces us to perform a basis transformation on the angular part of at least one side for each interface.

We considered two methods. One method is to use as a basis the Mathieu functions $C_k(q,\cdot)$ and $S_k(q,\cdot)$ for the value of q on one of the two sides of the interface. Since these Mathieu functions are orthonormal with respect to the standard L^2 inner product given by

$$\langle f, g\rangle = \frac{1}{\pi}\int_0^{2\pi} f(t)g(t)dt,$$

we can find the expansion of the functions $C_k(q',\cdot)$ and $S_k(q',\cdot)$ in this basis by simply calculating the inner products $\langle C_k(q',\cdot), C_l(q,\cdot)\rangle$ and $\langle S_k(q',\cdot), S_l(q,\cdot)\rangle$ (since arguments of oddness of the integrand show that $\langle C_k(q',\cdot), S_l(q,\cdot)\rangle = 0$). Unfortunately, not much is known about the coefficients obtained in this way.

Another method is to express both sets of solutions in the basis given by cosines and sines. The advantage is that the expansion of the angular Mathieu functions in cosines and sines has been studied previously. The disadvantage is that we now have to perform two basis transformations, which implies we make approximation/numerical errors twice. We will expand on this method further (the analysis of the first method is quite similar).

We need to find an expansion

$$C_k(q,x) = \sum_{j=0}^{\infty} c_j(k,q)\cos(jx),$$

where sines do not occur since $C_k(q,x)$ is even. Indeed, since C_k is either π-periodic or anti-periodic depending on the parity of k, only the $\cos(jx)$ occur where $k-j$ is even. Good algorithms to calculate these coefficients exist. Similarly we want the coefficients in

$$S_k(q,x) = \sum_{j=1}^{\infty} s_j(k,q)\sin(jx),$$

where again $s_j(k,q) = 0$ if $k-j$ is odd.

We remark that most of these coefficients are quite small, namely both $c_j(k,q) = O(\frac{q^{|k-j|/2}}{k^{|k-j|/2}})$ and $s_j(k,q) = O(\frac{q^{|k-j|/2}}{k^{|k-j|/2}})$ for fixed k, with small constants. For the specific values of q encountered in this problem we can therefore approximate $C_k(q,x)$ very well by $\cos(kx)$ for large enough k (for example $c_{k-2}(k,q) = q/4(k-1) + O(\frac{q^3}{k^3})$ if $k > 2$).

Matching the solution on each interface can now be done by equating the coefficients of each $\cos(jx)$ and $\sin(jx)$. For example, for the continuity on the interface between the second and third

layer we obtain

$$\sum_k [\alpha_{k,2} C(\lambda_k(q_2), q_2, -i\xi_3) + \beta_{k,2} S(\lambda_k(q_2), q_2, -i\xi_3)] c_j(k, q_2) = \sum_k \alpha_{k,3} C(\lambda_k(q_3), q_3, -i\xi_3) c_j(k, q_3),$$

as a relation between the coefficients of $\cos(jx)$ on both sides of the interface (recall that $\beta_{k,3} = 0$). Similarly the continuous radial differentiability at the interface gives us the relation

$$\sum_k [\alpha_{k,2} C'(\lambda_k(q_2), q_2, -i\xi_3) + \beta_{k,2} S'(\lambda_k(q_2), q_2, -i\xi_3)] c_j(k, q_2) = \sum_k \alpha_{k,3} C'(\lambda_k(q_3), q_3, -i\xi_3) c_j(k, q_3),$$

where the C' and S' are the derivatives of the radial solution.

In order to take F into account we will have to express that solution also in terms of cosines and sines on the interfaces. Since the solution F is generally not immediately given in terms of elliptical coordinates, there is no simple formula expanding this function in terms of cosines and sines. However we can always numerically calculate the Fourier coefficients to express

$$F(\xi_2, \eta) = \sum_j \psi_{j,2c} \cos(j\eta) + \psi_{j,2s} \sin(j\eta),$$

and a similar equation on the outer boundary.

If the assumption that the circular outer boundary can be approximated by an ellipse of sufficiently low eccentricity fails we can also use a similar calculation to express the basis functions of the solution on region I in terms of Fourier coefficients on an actual circle. However, calculating these coefficients involves (numerically) calculating many integrals for each basis function, and since each integral involves the slightly intractable Mathieu functions this could become computationally expensive.

Note that the resulting system of equations splits in four systems of equations. Indeed, we have one set of equations relating the $\alpha_{k,i}$ and $\beta_{k,i}$ for even k, one set for $\alpha_{k,i}$ and $\beta_{k,i}$ with odd k, one set for $\gamma_{k,i}$ and $\delta_{k,i}$ with even k and one set for $\gamma_{k,i}$ and $\delta_{k,i}$ with odd k. These sets of equations correspond to solutions which are even/odd in η (i.e. symmetrical or anti-symmetrical with respect to reflection in the horizontal axis) and π periodic/anti-periodic (i.e. symmetrical or anti-symmetrical with respect to the vertical axis). Since all sets are very similar we will focus on the first one.

5.3 Approximation

In order to obtain a finite set of equations we only consider a small number K of modes. This means we set $\alpha_{k,i} = 0$ and $\beta_{k,i} = 0$ for $k \geq K$. Note that here we only consider the equations between the $\alpha_{k,i}$ and $\beta_{k,i}$ with k even (as announced in the previous section), so in particular we forget about $\gamma_{k,i}$ and $\delta_{k,i}$. To obtain a system with the right amount of equations we moreover only consider the equations related to the coefficients of $\cos(jx)$ with $j \leq K$. Indeed, in the equations of the coefficient of $\cos(jx)$ for $j > K$ the terms with $\alpha_{j,i}$ are very dominant since $c_j(j, q_i) \approx 1$, while $c_j(k, q_i) \ll 1$ for $k \neq j$ and $j > K$, so including that equation without including the $\alpha_{j,i}$ term would probably lead to very bad results.

We now have to solve the system of equations

$$\begin{pmatrix} A_1(\xi_3) & 0 & 0 \\ A_1(\xi_2) & -A_2(\xi_2) & 0 \\ 0 & A_2(\xi_3) & -A_3(\xi_3) \\ A_1'(\xi_2) & -A_2'(\xi_3) & 0 \\ 0 & A_2'(\xi_3) & -A_3'(\xi_3) \end{pmatrix} \begin{pmatrix} \alpha_1 \\ \beta_1 \\ \alpha_2 \\ \beta_2 \\ \alpha_3 \end{pmatrix} = \begin{pmatrix} -F(\xi_3) \\ -F(\xi_2) \\ 0 \\ -F'(\xi_2) \\ 0 \end{pmatrix}.$$

Here $A_m(\xi_n)$ denotes the matrix

$$A_m(\xi_n) = \{C(\lambda_k(q_m), q_m, -i\xi_n)c_j(k, q_m), S(\lambda_k(q_m), q_m, -i\xi_n)c_j(k, q_m)\}_{0\le k,j\le K,\ k,j \text{ even}}$$

and similarly for $A_m(\xi_n)'$ (containing the derivatives of C and S). Moreover

$$\alpha_n = (\alpha_{n,k})_{0\le k\le K,\ k \text{ even}},$$

and finally

$$-F(\xi_n) = (-\psi_{j,nc})_{0\le j\le K,\ j \text{ even}}.$$

The problem thus involves solving a system of $5\lfloor (k+1)/2 \rfloor$ equations in as many variables. Considering the matrix is nearly sparse (i.e. involves many small terms as $c_l(k, q)$ is small for $|l-k| > 0$) this should be feasible, but we have not implemented it.

A numerical problem might occur since the columns in the matrix corresponding to $\alpha_{1,k}$ and $\beta_{1,k}$ are nearly identical, so the matrix becomes almost singular and likewise for $\alpha_{2,k}$ and $\beta_{2,k}$. The problem is that $C(\lambda_k(q), q, -i\xi)$ and $S(\lambda_k(q), q, -i\xi)$ (the basis of the solutions to the radial Mathieu equation) are very similar for large ξ. Indeed they are the generalizations of the hyperbolic cosines and sines, which both behave as $\exp(x)/2$ for large x. While $C(\lambda_k(q), q, -i\xi)$ and $S(\lambda_k(q), q, -i\xi)$ do not behave like $\exp(\xi)/2$ for large ξ, they still are very similar. In order to find a less near-singular matrix it would therefore be good to find a different basis of the radial solution to the Mathieu equations. Indeed the arguments given above apply to any basis of solutions (in the radial part), so the method would not need to change.

One convenient basis would be the one which intuitively is associated to $\exp(x)$ and $\exp(-x)$, namely $C(\lambda_k(q), q, -i\xi) + S(\lambda_k(q), q, -i\xi)$ and $C(\lambda_k(q), q, -i\xi) - S(\lambda_k(q), q, -i\xi)$. Unfortunately we have been unable to find any good algorithms to actually calculate these functions (other than calculating C and S and taking their difference, which does not behave well numerically as the difference of these two functions is much smaller than their values itself).

6 Optimization

We continue our semi-explicit approach to the problem and consider here the task of making the field in the patient as uniform as possible. We combine the separation-of-variables method in polar coordinates (i.e., using Bessel functions) from Section 4, with the handling of the boundary conditions between regions from Section 5. In particular, we use a discrete Fourier transform technique to match the solutions in the different regions at their common boundaries. Furthermore, we refrain from "normalizing" the Bessel functions (as was done in Section 4). Instead, we precondition the matrix that governs the matching of the Fourier modes, which reduces rank deficiencies (mentioned in Sections 4 and 5).

More precisely, *for each of the N antennas*, uniformly distributed on a circle of radius R_{ant}, we solve the Helmholtz equation with source term (3.5) using $2M + 1$ angular modes in the Fourier-Bessel expansion in each region (and correspondingly also $2M + 1$ modes in the Fourier expansion for the matching conditions at the boundaries), i.e.,

$$A = \sum_{m=-M}^{M} \left(a_{k,m} J_m(\zeta_k r) + b_{k,m} Y_m(\zeta_k r)\right) e^{im\theta},$$

for the three regions $k = 1, 2, 3$. We will only consider optimization of the field in (a subregion of) the core of the patient (region III). There, only Bessel functions of the first kind contribute ($b_{3,m} = 0$), and for the j^{th} antenna we denote the coefficients $a_{3,m}$ from now on by a_m^j. In region III, the expression for the potential then becomes

$$A = \sum_{l=1}^{N} c_l \sum_{m=-M}^{M} a_m^l J_m(\zeta r) e^{im\theta}, \tag{6.1}$$

where $\zeta = \zeta_3$, and the complex amplitudes $c_l = \mu_0 I_l$ appear as complex control parameters.

The magnetic field corresponding to A is given by

$$B = \begin{pmatrix} B^x \\ B^y \\ 0 \end{pmatrix} = \nabla \times \begin{pmatrix} 0 \\ 0 \\ A \end{pmatrix} = \begin{pmatrix} \frac{\partial A}{\partial y} \\ -\frac{\partial A}{\partial x} \\ 0 \end{pmatrix}.$$

The part of the field that we are interested in is $B^+ = B^x + iB^y$, since this is the (polarized) combination that turns the spins. This field, induced by the antennas, is often called B_1^+ to distinguish it from the much bigger constant field B_0 in the axial direction (generated by the superconducting magnet). We are thus interested in

$$B^+ = B^x + iB^y = \frac{\partial A}{\partial y} - i\frac{\partial A}{\partial x} = e^{i\theta}\left(\frac{1}{r}\frac{\partial A}{\partial \theta} - i\frac{\partial A}{\partial r}\right).$$

Using the identities

$$J_{m-1}(r) + J_{m+1}(r) = \frac{2m}{r} J_m(r), \qquad \text{and}$$
$$J_{m-1}(r) - J_{m+1}(r) = 2\frac{dJ_m}{dr}(r),$$

for Bessel functions, the expression (6.1) for the potential implies that the approximation of B^+ in the inner region III is

$$B^+ = \sum_{l=1}^{N} c_l \sum_{m=-M}^{M} i\zeta a_m^l J_{m+1}(\zeta r) e^{i(m+1)\theta}. \tag{6.2}$$

We have attempted to find those values of c_l for which B^+, rather than $|B^+|$, is as uniformly distributed as possible. We make this choice because this problem is *much* easier to solve and still leads to reasonably uniform $|B^+|$. The reason it is easier is that minimizing the variation in B^+, as formulated below, is in essence a least square problem, i.e., a *linear* algebra problem, while minimizing the variation in $|B^+|$ is a fully *nonlinear* optimization problem. Even if one eventually would like to optimize $|B^+|$, it would not be a bad idea to start that optimization procedure from

the easily computable configuration that optimizes B^+. Let us also remark that, to keep the method tractable, we did not consider the issue of minimizing the electric field.

Recalling that $\fint_\Omega B^+ = \int_\Omega B^+ / \int_\Omega 1$ is the average of B^+ on Ω, a simple and apparently satisfying approach is to use

$$\frac{\fint_\Omega \left|B^+ - \fint_\Omega B^+\right|^2}{\left|\fint_\Omega B^+\right|^2}$$

as a measure for the variation in B^+. We can rewrite this as

$$\frac{\fint_\Omega \left|B^+ - \fint_\Omega B^+\right|^2}{\left|\fint_\Omega B^+\right|^2} = \frac{\fint_\Omega |B^+|^2}{\left|\fint_\Omega B^+\right|^2} - 1.$$

Since this expression is clearly invariant under scalings of B^+, and since $\int_\Omega 1$ is just the (fixed) measure of Ω, one may reformulate the problem as finding the minimizer of

$$\min\left\{\int_\Omega |B^+|^2 \,:\, \fint_\Omega B^+ = 1\right\},$$

i.e., minimization is over all c_l such that $\fint_\Omega B^+ = 1$.

We first consider the case where the optimization domain Ω is a disk D of radius ρ around the origin, where ρ is sufficiently small, so that the domain lies entirely in region III. This choice of domain reduces the integral formulas considerably (we will review the general case below). In view of (6.2) the constraint becomes

$$\fint_\Omega B^+ = \frac{2}{\rho^2}\sum_{l=1}^{N} c_l a^l_{-1} i\zeta \int_0^\rho J_0(\zeta r) r\, dr = 1.$$

The expression to be minimized reduces to (complex conjugation denoted by a star)

$$\begin{aligned}\int_D |B^+|^2 &= \sum_{l,k,m,n} c_l c_k^* a^l_m a^{k*}_n \zeta\zeta^* \int_D J_{m+1}(\zeta r) J^*_{n+1}(\zeta r) e^{i(m+1)\theta} e^{-i(n+1)\theta} \\ &= \sum_{l,k,m} c_l c_k^* a^l_m a^{k*}_m \zeta\zeta^* 2\pi \int_0^\rho |J_{m+1}(\zeta r)|^2 r\, dr \\ &= \sum_{m=-M}^{M} \left| \sum_{l=1}^{N} c_l a^l_m \zeta \sqrt{2\pi \int_0^\rho |J_{m+1}(\zeta r)|^2 r\, dr} \right|^2 .\end{aligned}$$

To ease notation we introduce

$$q_{ml} = a^l_m \zeta \sqrt{2\pi \int_0^\rho |J_{m+1}(\zeta r)|^2 r\, dr},$$

and the matrix $Q = (q_{ml})$, as well as the vector $c = (c_l)$. Then

$$\int_D |B^+|^2 = \sum_m \left| \sum_l c_l q_{ml} \right|^2 = |Qc|^2 .$$

To write the constraint in linear algebra terms as well, define the vector $p = (p_l)$ with

$$p_l = \tfrac{2}{\rho^2} a^l_{-1} i\zeta \int_0^\rho J_0(\zeta r) r\, dr.$$

Then we may reformulate the problem as finding the least-square solution of $Qc = 0$ under the constraint $p^T c = 1$.

With a final reformulating step the constraint can be absorbed into the matrix, namely define

$$\tilde{Q} = \begin{pmatrix} p^T \\ Q \end{pmatrix},$$

and let e_1 be the standard unit vector. Find the least-square solution of $\tilde{Q}x = e_1$, say $x = \tilde{c} = (\tilde{c}_l)$, then, using the linearity of the problem, it follows that the optimal $c = (c_l)$ of the constraint problem above is given by a rescaled version of $\tilde{c}$, namely

$$c_l = \frac{1}{p^T \tilde{c}} \tilde{c}_l.$$

For general domains Ω this can be generalized as follows. Let us describe the method for a two-dimensional integral using polar coordinates, but it is straightforward to extend. We first want to discretize the integral. Let Ω lie inside some (large) disk D_R, and let Δr and $\Delta\theta$ be discretization step sizes, so that $n_1 = \frac{R}{\Delta r}$ and $n_2 = \frac{2\pi}{\Delta\theta}$ are integers. The grid points are now given by $r^{j_1} = (j_1 - \frac{1}{2})\Delta r$ and $\theta^{j_2} = j_2 \Delta\theta$ for $1 \le j_1 \le n_1, 1 \le j_2 \le n_2$. Let I be an enumeration of all the grid points that lie *inside* Ω, and $1 \le i \le N_\Omega$ (with $N_\Omega \le n_1 n_2$) indexes I, i.e., $(r_i, \theta_i) \in \Omega$.[5] Then

$$\int_\Omega f(r,\theta) \approx \Delta r \Delta\theta \sum_{i=1}^{N_\Omega} f(r_i, \theta_i) r_i,$$

where the final "weight" r_i is due to the polar-coordinate Jacobian. With this discretization in place, we may write, with $\delta = \Delta r \Delta\theta$

$$\int_\Omega |B^+|^2 \approx \sum_{l,k,m,n,i} c_l c^*_k a^l_m a^{k*}_n |\zeta|^2 \delta J_{m+1}(\zeta r_i) J^*_{n+1}(\zeta r_i) r_i e^{i(m+1)\theta_i} e^{-i(n+1)\theta_i}.$$

To simplify notation we introduce

$$g_{im} = J_{m+1}(\zeta r_i) e^{i(m+1)\theta_i} \sqrt{r_i \delta},$$

and the matrix $G = (g_{im})$, as well as $h_{ml} = a^l_m \zeta$ and $H = (h_{ml})$. Then the above expression reduces to

$$\int_\Omega |B^+|^2 \approx \sum_{l,k,m,n,i} c_l c^*_k h_{ml} h^*_{nk} g_{im} g^*_{in} = \sum_i \left| \sum_{m,l} g_{im} h_{ml} c_l \right|^2 = |GHc|^2.$$

The remainder of the argument is now analogous (with $Q = GH$) to the case $\Omega = D$.

[5] A formal description is as follows: let $I = \{(j_1, j_2) \,|\, (r_{j_1}, \theta_{j_2}) \in \Omega\}$, and N_Ω is the number of elements in the set I. Then there are "enumeration" functions $\tilde{\jmath}_1(i)$ and $\tilde{\jmath}_2(i)$ such that $I = \{(\tilde{\jmath}_1(i), \tilde{\jmath}_2(i)) \,|\, 1 \le i \le N_\Omega\}$. Now set $r_i = r^{\tilde{\jmath}_1(i)}$ and $\theta_i = \theta^{\tilde{\jmath}_1(i)}$.

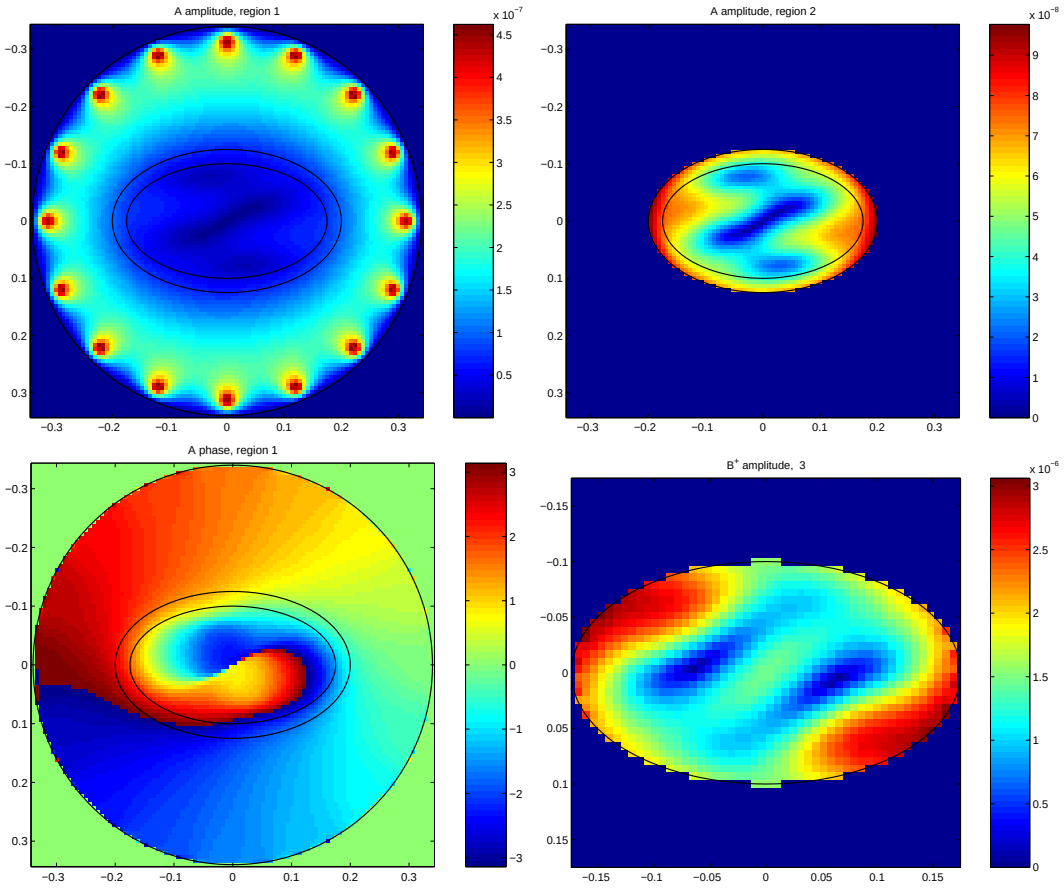

Figure 6.1: The amplitude and phase of the fields A and B^+ in the different regions. The antenna currents are *not* optimized.

6.1 Results

The computational parameters in the simulation were chosen as follows: 65 Fourier-Bessel modes are used in each region (for both types of Bessel functions), and 2^8 discretization points on each boundary. The optimization computation in this case only takes a few seconds. For the physical parameters we used realistic values provided by the problem presenters: $\epsilon_2 = 10\epsilon_0$ and $\sigma_2 = 0.076$ for the fatty layer, and $\epsilon_3 = 34\epsilon_0$ and $\sigma_3 = 0.4$ for the interior part of the body. The parameters that determine the geometry of the MRI scanner are the same as in Section 4. Note that since the problem is linear the absolute size of the fields is fairly irrelevant (although it is of course important in practice), since it can be tuned by an arbitrary multiplicative constant.

For comparison, we first look at the non-optimized fields in Figure 6.1. There the amplitudes of the currents in the antennas are all equal and the phase is rotated uniformly ($I_l = I_1 e^{2\pi i(l-1)/16}$). We indeed see the phase of A nicely rotating, while the field does not penetrate the body very well. Looking at the crucial B^+ field, we see that its amplitude is nonuniform and very small in certain central parts of the body.

In Figure 6.2 we have optimized (in the sense explained above) the B^+ field in a disk of radius

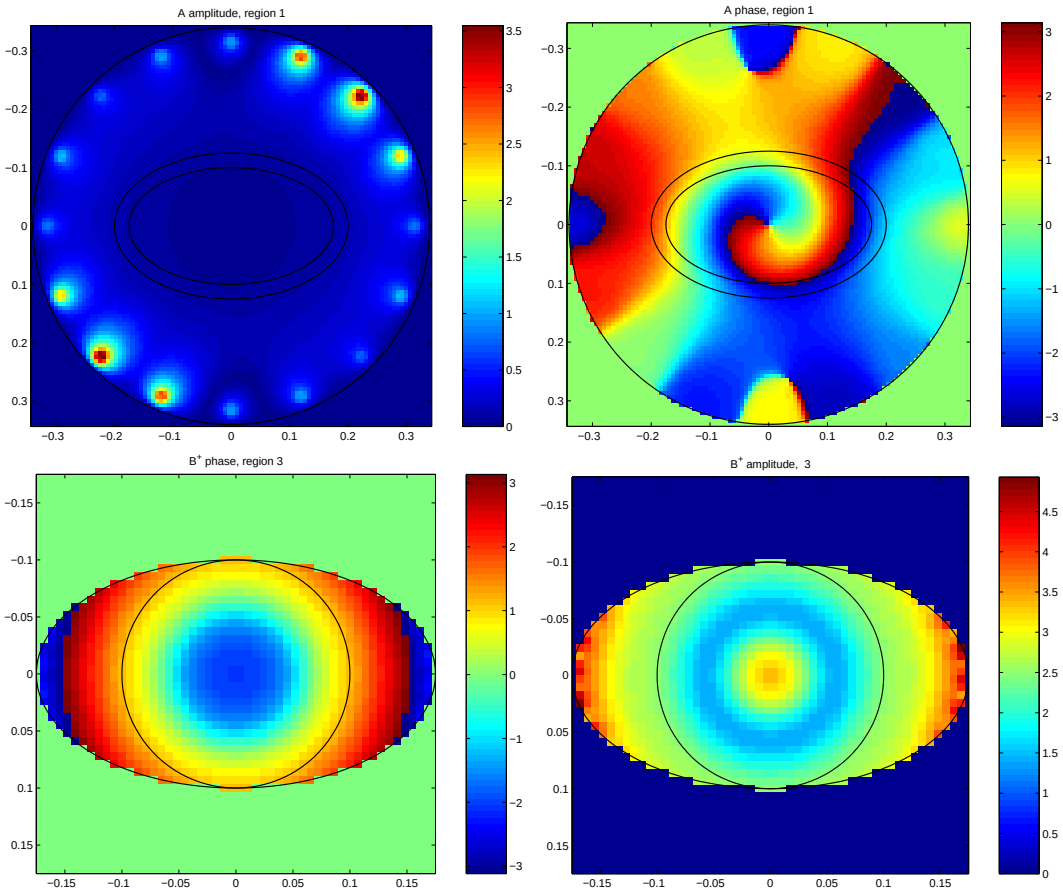

Figure 6.2: The amplitude and phase of the fields A and B^+ in the different regions. The antenna currents are optimized as to make B^+ optimally uniform in the indicated disk inside the inner ellipse.

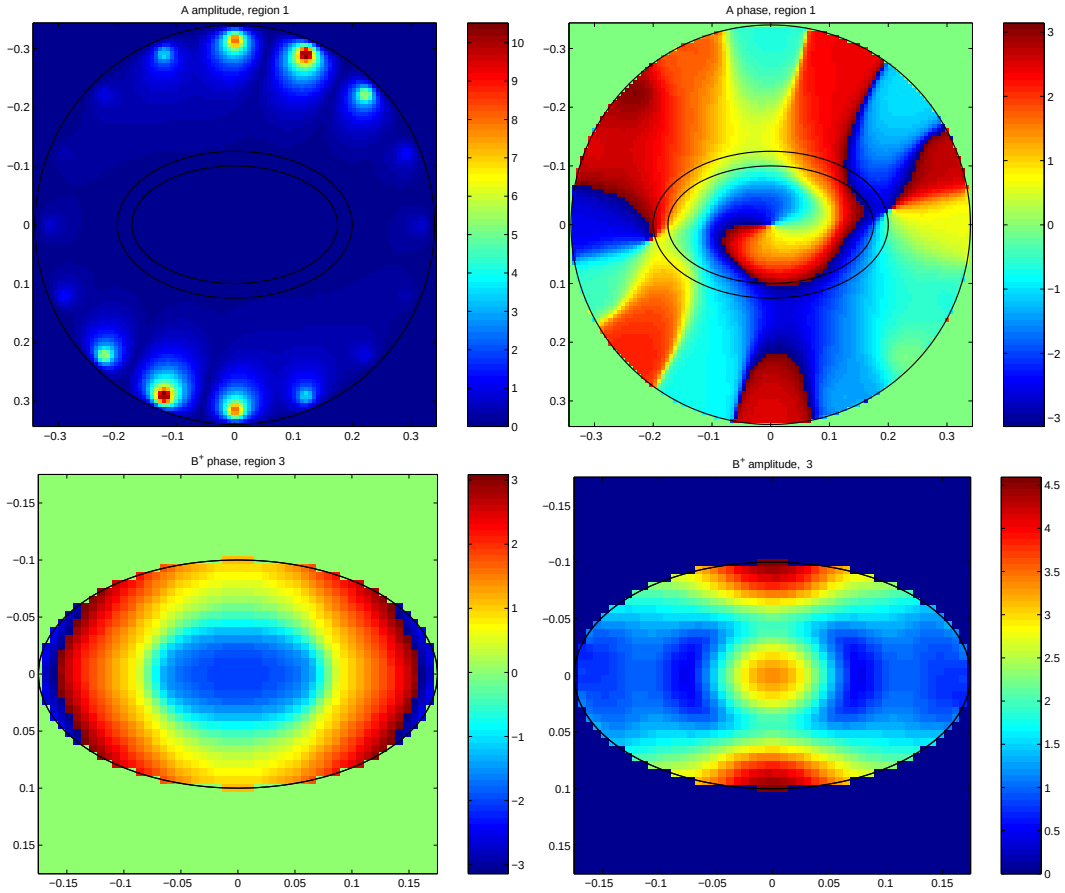

Figure 6.3: The amplitude and phase of the fields A and B^+ in the different regions. The antenna currents are optimized as to make B^+ optimally uniform in the entire inner ellipse.

0.1 m around the origin (the optimization region is indicated in the figure). We see that although our method makes B^+ optimally uniform, in fact the amplitude $|B^+|$ is much more uniform than the phase. This is a bit unexpected, but it is very welcome in view of the original aim of making this amplitude uniform, and we are pleasantly surprised by how uniform the amplitude of the field is: the fluctuations are within a factor 2. When we look at the antennas, we see quite a spread in current amplitudes, and the complicated phase pattern illustrates the subtleness of the optimal configuration.

Next we optimize the B^+ field on the entire inner ellipse (the interesting not-fat part of the body). In Figure 6.3 we see that the amplitude of the resulting field is less uniform, which is to be expected since we are trying to make it uniform on a bigger domain, but the results are still much better than the non-optimized case in Figure 6.1.

Finally, we optimize on a domain whose size is in between the disk and the entire ellipse. The results are depicted in Figure 6.4, where also the domain of optimization is indicated. The results show a fairly uniform $|B^+|$: within a factor 3 over the entire ellipse representing the inner region of the body. This demonstrates that the relatively simple optimization procedure performs satisfactorily even on non-circular domains. We note however that perhaps the optimization in Figure 6.2 is

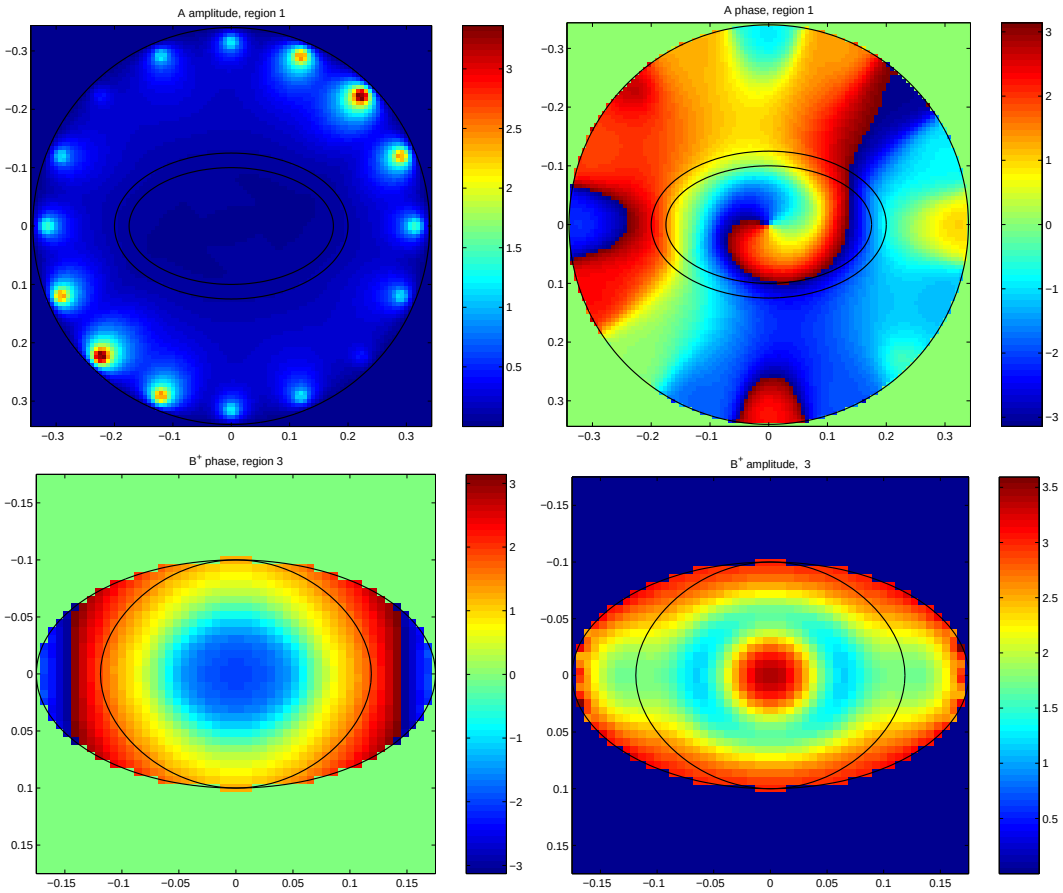

Figure 6.4: The amplitude and phase of the fields A and B^+ in the different regions. The antenna currents are optimized as to make B^+ optimally uniform in the indicated domain.

preferable. Furthermore, the pattern in the (amplitude and phase of) antenna currents is quite similar to Figure 6.2.

7 Concluding remarks

After completing the report we asked Ir. Bob van den Bergen and Dr. Ir. Nico van den Berg of the Department of Radiotherapy of the University Medical Center in Utrecht to write the concluding remarks on the results obtained for the problem they submitted to the study group:

The UMC Utrecht problem consisted of finding a semi-analytical method to calculate and optimize rapidly the radiofrequency (RF) field of an MRI scanner. According to the UMC Utrecht this goal has been fully achieved. The developed model allows an evaluation of the full electromagnetic field in less than a minute. This enables an on-the-fly optimization procedure for patients. At the moment we are designing the RF hardware to implement this procedure for our 7 Tesla MRI scanner.

As an extra bonus we obtained a rapid optimization method which is based on a simple least squares method in stead of the conventionally applied non-linear optimization procedures which suffer from lengthy calculation times and local minima. Currently, we are using this to study the ultimate RF homogeneity as a function of various physical parameters. Furthermore, the short computation time opens up the new possibility to find the optimal coil geometry in an automated fashion. Concluding, we can state that the SWI workshop has been a great success for the UMC Utrecht and has resulted in much new research.

The UMC Utrecht would like to express their gratitude for being able to take part in this workshop. It is quite unique that such mathematical talent and knowledge is brought together to solve such a complex modelling problem in the medical industry. The rigorous mathematical methodology of the participants applied to this physical problem has been an eye-opener. On a more personal level, we would like to thank to all the participants for their work and great character. Enlighten all these mathematical heathens out there!

Acknowledgments

There are plenty of people to thank for their help. First of all we thank the organizers for providing a comfortable atmosphere and an inspiring program. We also thank Nico van den Berg and Bob van den Bergen (from the UMC Utrecht) for proposing this stimulating problem, and for their ceaseless patience and good humor. We also thank experts Hans Duistermaat and Ernst van Faassen, for their comments on PDEs and Maxwell theory, respectively. Finally, the participants thank each other for the enthusiastic cooperation and good spirit which characterized the week.

References

[1] J. D. Jackson. Classical electrodynamics, 3rd ed. John Wiley & Sons, Inc, 1999.

[2] E. Mathieu. Mémoire sur le mouvement vibratoire d'une membrane de forme elliptique. *Jour. de Math. Pures et Appliquées*, 13:137–203, 1868.

[3] J. C. Gutiérrez Vega. Theory and numerical analysis of the Mathieu functions. *Lecture notes*, Monterrey, 2003.

[4] J. C. Gutiérrez Vega, R. M. Rodríguez-Dagnino, M. A. Meneses-Nava, S. Chávez-Cerda. Mathieu functions, a visual approach. *Am. J. Phys.*, 71(3): 233–242, 2003.

[5] http://www.fcc.gov/cgi-bin/dielec.sh